

Interannual Variability of Indian Ocean Heat Transport

GALINA CHIROKOVA

Program in Atmospheric and Oceanic Sciences, University of Colorado, Boulder, Colorado

PETER J. WEBSTER

Schools of Earth and Atmospheric Sciences, and Civil and Environmental Engineering, Georgia Institute of Technology, Atlanta, Georgia

(Manuscript received 5 November 2003, in final form 6 September 2005)

ABSTRACT

The work in this paper builds upon the relatively well-studied seasonal cycle of the Indian Ocean heat transport by investigating its interannual variability over a 41-yr period (1958–98). An intermediate, two-and-a-half-layer thermodynamically active ocean model with mixed layer physics is used in the investigation. The results of the study reveal that the Indian Ocean heat transport possesses strong variability at all time scales from intraseasonal (10–90 days) to interannual (more than one year). The seasonal cycle dominates the variability at all latitudes, the amplitude of the intraseasonal variability is similar to the seasonal cycle, and the amplitude of the interannual variability is about one-tenth of the seasonal cycle. Spectral analysis shows that a significant broadband biennial component in the interannual variability exists with considerable coherence in sign across the equator. While the mean annual heat transport shows a strong maximum between 10° and 20°S, interannual variability is relatively uniform over a broad latitudinal domain between 15°N and 10°S. The heat transport variability at all time scales is well explained by the Ekman heat transport, with especially good correlations at the intraseasonal time scales. The addition of the Indonesian Throughflow does not significantly affect the heat transport variability in the northern part of the ocean.

1. Introduction

The Asian–Australian monsoon is a coupled ocean–atmosphere–land phenomenon with an intensity that is regulated through negative feedbacks between the land, ocean, and atmosphere (e.g., Webster et al. 1998, 2002b; Loschnigg et al. 2003). The ocean component of the coupled system is arguably the least well known, in particular its interannual variability.

A number of studies have calculated the mean annual heat transport and the mean seasonal cycle of the heat transport in the Indian Ocean. The methods used include calculation of the oceanic heat budget as a residual from atmospheric measurements (Hsiung et al. 1989; Trenberth and Solomon 1994), estimation from the hydrographic data (Hastenrath and Lamb 1980; Fu

1986; Hastenrath and Greischar 1993), and modeling studies (Waengne and Pacanowski 1996; Garternicht and Schott 1997; Lee and Marotzke 1997, 1998; Jayne and Marotzke 2001). Despite limitations and different errors inherent to each method, all mentioned above studies are in a good agreement. Figure 1 compares estimates of the seasonal cycle of a number of studies. Specifically, Fig. 1a shows model estimates of the latitudinal distribution of heat transport as a function of time from Waengne and Pacanowski (1996), Figs. 1b,c show estimates from residual techniques and available hydrographic data (Hsiung et al. 1989; Hastenrath and Greischar 1993), and Fig. 1d shows the transport distribution from the model used in this study (see section 2). The four studies show the same general distributions of heat transport; that is, a large southward transport (−1.5 to −2 PW) between spring and fall and a northward transport (+1.5 to +2 PW) during the rest of the year. Furthermore, all estimates show a maximum heat transport on the south side of the equator between 10° and 15°S. Each heat transport distribution is also con-

Corresponding author address: Galina Chirokova, Program in Atmospheric and Oceanic Sciences, University of Colorado, UCB 311, Boulder, CO 80302.
E-mail: galka@enso.colorado.edu

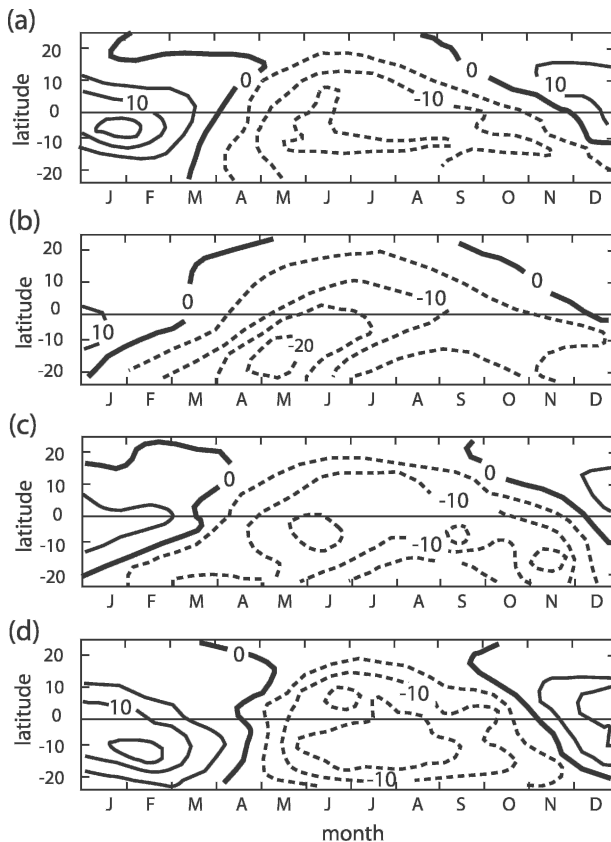


FIG. 1. Comparison of estimates of the seasonal cycle of the meridional heat transport by (a) Wacongne and Pacanowski (1996), (b) Hsiung et al. (1989), (c) Hastenrath and Greischar (1993), and (d) the current study using the model described in section 2. (Units: 0.1 PW.)

sistent with the annual cycle of wind-driven Ekman heat transport discussed earlier by several authors (e.g., Levitus 1987; Loschnigg and Webster 2000; Jayne and Marotzke 2001).

In addition to the strong seasonal cycle, there is much evidence of a strong aperiodic and high-amplitude atmospheric and oceanic variability on intraseasonal, biennial, and interannual time scales over the Indian Ocean (see review by Webster et al. 1998). Han et al. (2001) found $\pm 1\text{--}2$ PW heat transport changes in response to intraseasonal wind forcing. Biennial variability has been studied by several authors (see Meehl 1987, 1997; Goswami 1995; Clarke et al. 1998, among others). Five-year variability has also been identified by Nicholson and Nyenzi (1990) and Terray (1995).

There is recent evidence that the Indian Ocean possesses modes that are inherent to the basin and either act independently or are forced by remote forcing such as El Niño–Southern Oscillation (ENSO). This phenomenon is referred to as the Indian Ocean dipole or

the Indian Ocean Zonal Mode (IOZM; Webster et al. 1999; Saji et al. 1999; Anderson 1999; Yu and Rienecker 1999, 2000). The discovery of the IOZM resulted in a number of papers in recent years examining the interannual variability of the Indian Ocean. Among others are works by Murtugudde and Busalacchi (1999), Behera et al. (2000), and Huang and Kinter (2002). However, these papers mostly concentrated on surface observations, and mixed layer heat budget. Feng and Meyers (2003) analyzed the subsurface ocean dynamics based on observed sea level anomalies and temperature data. If the ocean is a critical element of regulation of the amplitude of the monsoon as suggested by Webster et al. (2002b) and Loschnigg et al. (2003), then there should be a recognizable interannual signal in heat transports that somehow matches the amplitude of the monsoon anomaly. It is difficult to assess this interannual variability observationally, because only occasional observational snapshots of internal processes are available [e.g., the Joint Air–Sea Monsoon Interaction Experiment (JASMIN); Webster et al. 2002a; or the Bay of Bengal Experiment (BOBMEX); Bhat et al. 2001] or measurements of surface characteristics from satellite. Therefore, the best available option for looking at variability of the ocean at this time will be to use an ocean model forced by atmospheric fields, which are relatively well known. Using this strategy, Loschnigg and Webster (2000) used a 7-yr Indian Ocean model run to study the interannual variability of the Indian Ocean heat transport and assess the variability in the North Indian Ocean (NIO) heat budget, where NIO is defined as the portion of the Indian Ocean north of the equator. Recently Jayne and Marotzke (2001) analyzed the interannual variability of the World Ocean heat transport for the years 1988–97, using the Parallel Ocean Climate Model. They presented an explanation of the heat transport variability, discussed the role of the variable wind stress and the connection between the heat transport variability and the Ekman transport, concluding that the Ekman heat transport and the physics underlying it is the key to understanding a large part of the time-varying heat transport. They also presented estimates of the heat transport variability for the global ocean.

In the current study, with the use of an intermediate ocean model, we produce a 41-yr (1958–98) evolution of the Indian Ocean heat budget. The budget is resolved at 5-day intervals. The relatively short temporal resolution and the length of the integrations allow the analysis of both interannual (longer than one year) and intraseasonal (from 10 to 90 days) variability. In the next section, we describe the model and the forcing used. In section 3, we present results of the model in-

tegrations. We discuss the seasonal cycle of the heat budget in the Indian Ocean, show that the heat transport undergoes strong variability at all time scales from intraseasonal to interannual, and determine the nature of the interannual variability, in particular its biennial nature. We also analyze the correlation between the Ekman transport and the heat transport at different time scales, and discuss how our results are affected by the addition of the Indonesian Throughflow (ITF) to the model. In section 4 we present conclusions.

2. Model, data, and methods

a. Model and model heat budget

The model used is a version of McCreary et al. (1993) two-and-a-half-layer Indian Ocean model with a mixed layer imbedded within the upper layer and a 55-km grid resolution. The model was developed by McCreary et al. (1993), and used in several studies (e.g., Loschnigg and Webster 2000; Behera et al. 2000) in which details of the model are presented. The temperatures of the two active layers can vary but salinity is not included. The entrainment and detrainment of water is allowed to account for the exchange of mass, momentum, and heat between layers. The model develops its own turbulent fluxes of sensible and latent heat from the imposed atmospheric forcing and the state of the upper layers of the ocean model. The mixed layer entrainment is governed by Kraus–Turner mixing conditions (Kraus and Turner 1967), in which mixing is maintained by turbulence generated at the surface by stirring and cooling. The southern boundary of the model does not correspond to any real boundary of the Indian Ocean, and the zero-gradient, open-boundary conditions are applied there. The model heat budget is calculated in the same way as in Loschnigg and Webster (2000). For the closed region as the NIO used in the model, where the ITF has been neglected, the model heat budget for a volume of the ocean is

$$Q_t = Q_v + Q_s + \text{diffusive terms}, \quad (1)$$

where Q_t is the change in heat storage, Q_v is the heat transport into the volume, and Q_s is the total net surface flux into the ocean. Diffusive terms are much smaller than other terms and are neglected in the current discussion. The rate of change of heat storage is defined as

$$Q_t(t) = \rho c_p \iiint \frac{\partial T}{\partial t} dx dy dz, \quad (2)$$

the surface heat flux into the ocean is

$$Q_s(t) = \iint (Q_{sw} + Q_{lw} + Q_{LE} + Q_{SH}) dx dy, \quad (3)$$

and the meridional heat transport is

$$Q_v(t) = \rho c_p \iint vT dx dz, \quad (4)$$

where Q_{sw} is the solar radiation, Q_{lw} is the outgoing longwave radiation, Q_{LE} is latent heat flux, Q_{SH} is sensible heat flux, and v and T are the meridional velocity and temperature, respectively. Longitude, latitude, and depth are represented by x , y , and z , respectively.

For the definition of the heat transport to be valid, there must be a zero net mass transport across the meridional section. For the model used in this study this is not true. The model formulation includes the requirement of the conservation of the total mass in the basin; however, the mass of the water north of any given latitude inside the basin is constantly changing. To take that into account, we calculate the heat transport following Hall and Bryden (1982) and Loschnigg and Webster (2000). We assume that the mass transport in the abyssal layer compensates for the mass transport in two upper layers; that is,

$$\int v_3 H_3 dx = - \int (v_1 H_1 + v_2 H_2) dx, \quad (5)$$

where v_i ($i = 1, 2, 3$) represents the meridional velocity component, and H_i represents the depth of the layers. For the layers having temperatures T_i , and the deep ocean temperature T_3 , the total heat transport is

$$\begin{aligned} Q_v &= \rho c_p \int_{i=1}^3 v_i H_i T_i dx \\ &= \rho c_p \int [v_1 H_1 (T_1 - T_3) + v_2 H_2 (T_2 - T_3)] dx. \end{aligned} \quad (6)$$

The deep ocean temperature (T_3) is taken to be 4°C (Levitus 1982).

b. Forcing of the ocean model

The ocean model was run for a 41-yr period (1958–98) driven by surface air temperature, surface winds, specific humidity, and net surface radiation from the National Centers for Environmental Prediction–National Center for Atmospheric Research (NCEP–NCAR) Reanalysis data (Kalnay et al. 1996; Kistler et al. 2001). The radiative forcing used in the model was obtained by correcting NCEP radiation fields to match the mean fluxes calculated from the surface radiation budget (SRB) dataset (Darnell et al. 1996), which is available

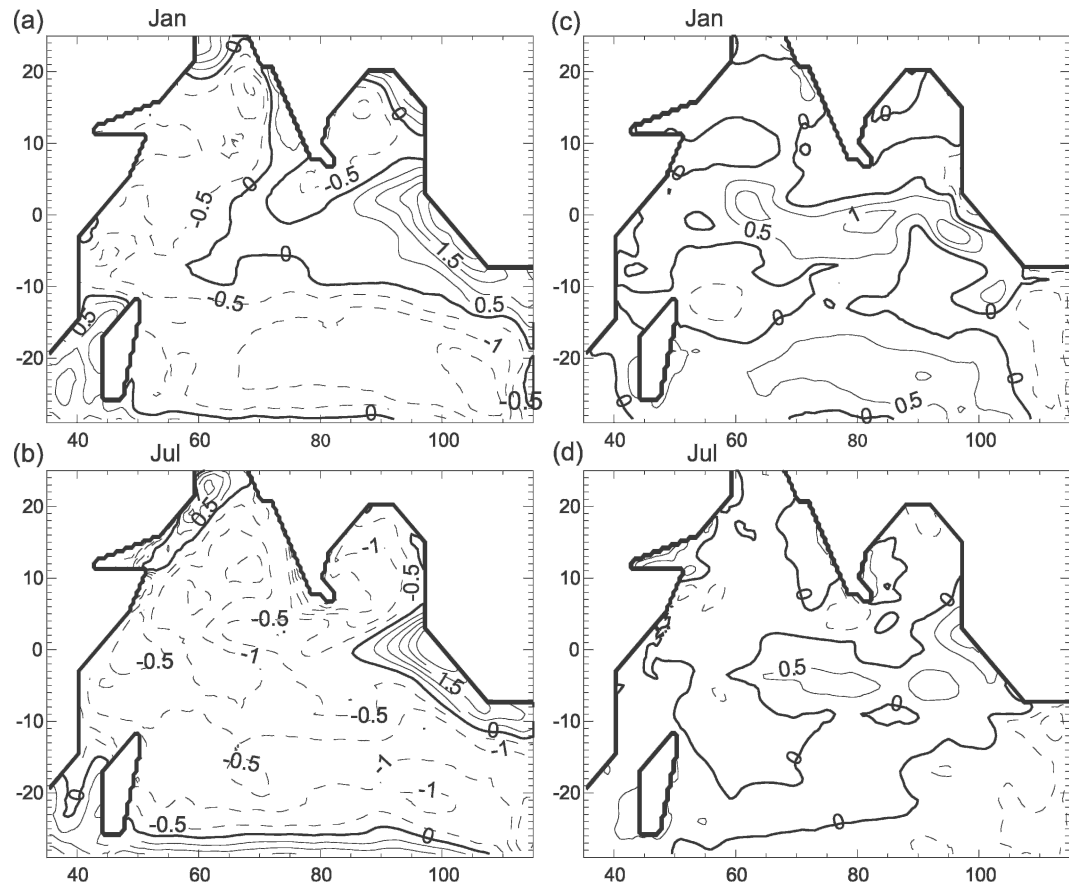


FIG. 2. (a), (b) Modeled-observed SST for January and July. Both estimates are averaged over the years 1958–98. (c), (d) Modeled-observed SST anomalies for January and July for the year 1987. Observed SST after Reynolds and Marisco (1992). (Units: °C.)

for the 7-yr period (1984–91; the data are available online at http://srblwlarc.nasa.gov/SRB_homepage.html). This radiative-forcing correction provides better agreement between model and observed SST data although, as it turns out, the model is far more sensitive to wind forcing than radiative forcing. Following Han and Webster (2002), the model was forced by the 90% NCEP–NCAR reanalysis 1000-mb wind stress to account for the logarithmic wind profile in the surface layer. The NCEP–NCAR reanalysis dataset was chosen because it comprises the longest homogeneous dataset currently available.

According to Kistler et al. (2001), the interannual variability of the reanalysis data tends to be correlated with independent observations. However, some caution should be used since the reanalysis data are influenced both by observations and by the model, and thus sometimes could differ substantially from observations. The NCEP–NCAR reanalysis provides daily averages on a T62 Gaussian grid. For our purposes, we average these

data every five days, producing 73 forcing fields for each year, and interpolate to the model 0.5° grid. Forcing fields of the ocean model were computed in this manner for the 41-yr period. Initially, the model was spun-up for 10 yr using mean annual cycle forcing obtained by averaging the 41-yr period. At year 10 the model circulation approaches stationarity. The last year of the spinup is used as initial conditions for the main model run.

Test runs with daily output show that the model does not produce any significant variability not present in the model forced by pentad fields. The model performance was tested against SST data. For this purpose Reynolds SST (Reynolds 1988; Reynolds and Marisco 1993) and Comprehensive Ocean–Atmosphere Data Set (COADS) SST data (Oberhuber 1988) were used. The model SST and SST anomalies compare well with the observational data. Figure 2 shows the comparison of the modeled SST to the Reynolds SST. The comparison is made for January and July. Figures 2a,b show

the difference between 41-yr-averaged model and Reynolds SST averaged over the same period. The corresponding root-mean-square errors (rmse) are 0.69 for January and 0.82 for July. Figures 2c,d show the difference between the modeled and observed SST anomalies for the year 1987. The corresponding rms errors are 0.35 for January and 0.29 for July. As could be seen, for the mean state for most part of the basin the difference does not exceed 1°C, and for the anomalies the difference is mostly below 0.5°C. A 41-yr integration with the same forcing for each year was performed to ensure that model results did not have any artificial drift resulting from the long-term integration. The comparison of the SST fields between the first and last years of the test run showed that the SST difference never exceeded 0.02°C, and did not show any consistent drift.

3. Results and discussion

First, we calculate the seasonal cycle of the Indian Ocean heat transport and compare it with the previous studies. This comparison allows us to estimate the reliability of the heat transport calculations from the model. Based on these estimates, we investigate the intraseasonal and interannual variability of the heat transport.

a. Seasonal cycle of the Indian Ocean heat budget

1) COMPARISON BETWEEN THE CURRENT MODEL AND PREVIOUS RESULTS

The mean seasonal cycle of the Indian Ocean heat transport, plotted as a function of latitude and month, is shown in Fig. 1d. The relatively simple two-and-a-half-layer model appears to agree well with other estimates of the seasonal cycle of the oceanic heat transport, shown in Figs. 1a–c. The similarity confirms that the heat transport calculations found in our integrations are independent of the particular choice of the model. The model used by Wacongne and Pacanowski (1996), as well as the model used in the current study, does not include the ITF. The very good agreement with the estimates from residual techniques (Hsiung et al. 1989) and hydrographic data (Hastenrath and Greischar 1993) suggests that the ITF is probably not crucial for the seasonal cycle of the heat transport at least to first order. Whether or not it is a more critical component of interannual variability is not known. We will discuss aspects of the ITF in section 3e.

There are, however, a number of limitations in using only a two-and-a-half-layer model. Miyama et al. (2003) point out that the net southward heat transport in the Indian Ocean is associated with the shallow cross-

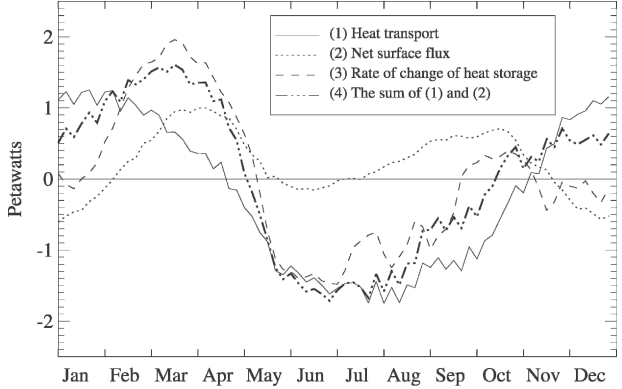


FIG. 3. Seasonal cycle of the components of the mean NIO heat balance: mean northward oceanic heat transport across the equator, the rate of change of heat storage of the upper 500 m of the NIO, net surface heat flux over the Indian Ocean north of the equator, and the sum of the net surface heat flux and heat transport. (Units: PW.)

equatorial meridional overturning cell, which is well resolved by two-and-a-half-layer model. However, as discussed by Schott and McCreary (2001) there is still considerable uncertainty related to the existence of the deep meridional overturning cell in the Indian Ocean, and whether such cell would affect the meridional heat transport. For example, Wacongne and Pacanowski (1996) found that during the northeast monsoon in the boreal winter most of the model heat transport is carried by a deep downwelling cell. Recently Ferron and Marotzke (2003) found that the deep overturning carries 10% of the total southward energy flux at 32°S.

2) THE SEASONAL CYCLE OF THE HEAT BALANCE OF THE NIO

Figure 3 shows the seasonal cycle of the components of the heat balance of the NIO as a function of time of year: the seasonal cycle of mean northward oceanic heat transport across the equator, the rate of change of heat storage of the upper 500 m of the NIO, the net surface heat flux over the Indian Ocean north of the equator, and the sum of the surface heat flux and heat transport. Similar computations were made by Loschnigg and Webster (2000), although they used the COADS climatology to obtain long-term average values.

For the cross-equatorial heat transport, the maximum amplitudes reached are 1.2 PW in January and –1.6 PW in July. The NIO heat storage change reaches a maximum value of 1.9 PW in March, and the minimum value of –1.4 PW in June. While heat transport and heat storage change have a strong annual component, the net surface heat flux has a strong semiannual component. The net surface heat flux is the sum of the

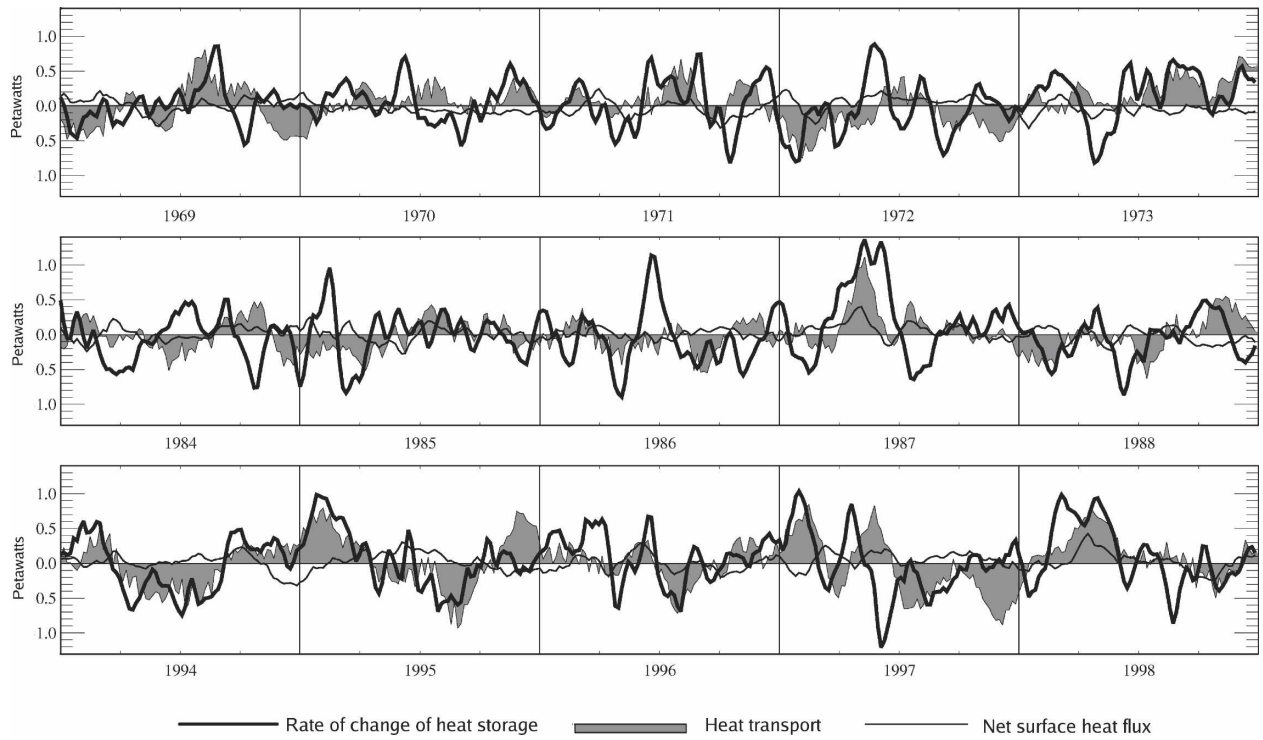


FIG. 4. Time series of the anomalies of the components of the heat budget for the years (top) 1969–73, (middle) 1984–88, and (bottom) 1994–98. The time series are smoothed with nine points running average for clarity and to isolate major lower frequency changes. The seasonal cycle is removed. Major anomalies occur at all times of the year. (Units: PW.)

longwave and shortwave radiation and sensible and latent heat fluxes. It has two positive peaks in March and October, reaching correspondingly 1.0 and 0.8 PW. These maximum values are reached during the transition time between winter and summer monsoons, as a result of the enhanced heating of the ocean during the boreal summer combined with the reduced winds. The net surface flux reaches minimum values of -0.6 PW in January and -0.15 PW in the midsummer (June). The minimum values of the net surface flux are reached at the peak of the winter and summer monsoon seasons. These minima can be explained by wind and solar radiation variability. During winter, the NIO has a minimum in solar radiation and moderate winds. During the boreal summer, solar radiation is reduced by increases in cloudiness and vertical mixing enhanced by very strong winds.

b. The relationship between the seasonal cycle and intraseasonal and interannual variability

1) COMPARISON BETWEEN THE CURRENT MODEL AND PREVIOUS RESULTS

The 41-yr model run, with the 5-day output, allows us to look at variability over a wide range of temporal

scales. Figure 4 shows the time series of the anomalies of the cross-equatorial heat transport, NIO heat storage change, and NIO surface flux. Time series shown on Fig. 4 are smoothed with a nine-point running average, and with the seasonal cycle removed. High-amplitude variability is evident on all time scales from 10 days to several years in both summer and winter. From Fig. 4 it appears that the intraseasonal variability of the heat transport does not have any preferred time of the year. For Fig. 4 we picked the years, which show that the amplitude of the intraseasonal signal may remain strong or weak for the whole year, or change significantly from one season to another. For example, in 1995 we can see strong heat transport anomalies at all seasons, whereas in 1970 the anomalies are low at all time. However, in 1987 and 1998 there are strong positive heat transport anomalies in spring and relatively small anomalies during the rest of the year. The amplitude of the short time variations in the heat transport could be as much as 1.5 PW, which is similar to the amplitude of the seasonal cycle. In fact, Jayne and Märtzke (2001) found for the global ocean heat transport that some short-term fluctuations near the equator can completely compensate the seasonal cycle. The Fourier spectrum of the unfiltered time series with the seasonal

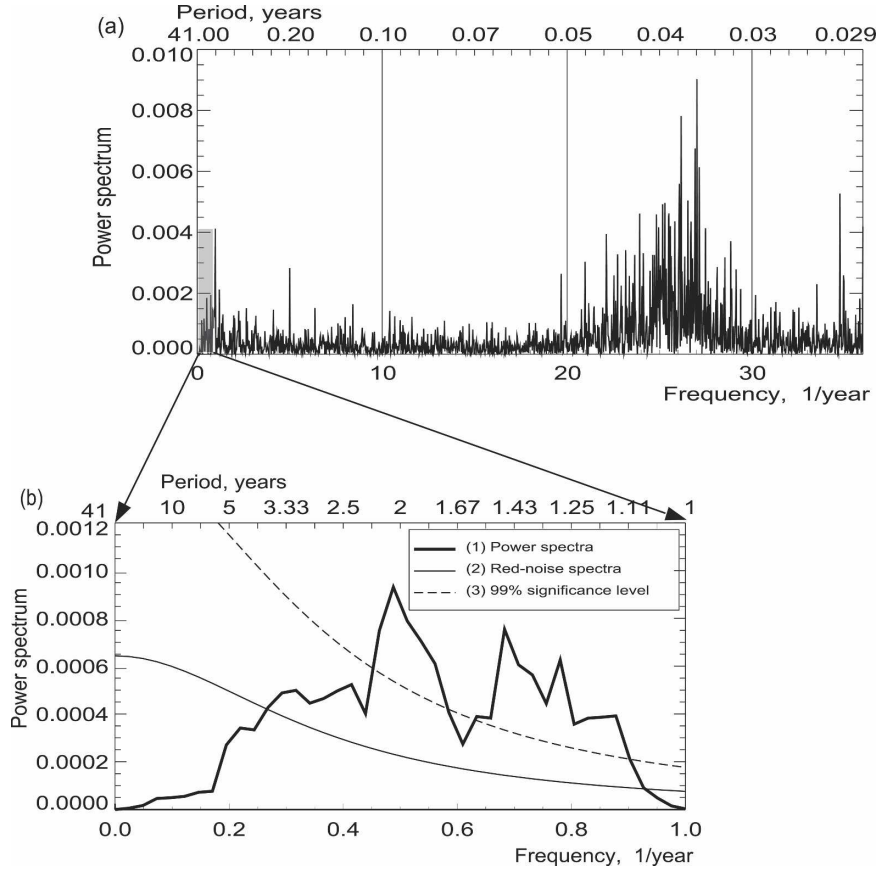


FIG. 5. (a) Unfiltered power spectrum of the cross-equatorial heat transport. The seasonal cycle is removed by excluding the first four annual harmonics. (b) Part of the spectrum corresponding to the shaded area in the lhs of (a). The seasonal cycle is removed by subtracting the first four annual harmonics. The 99% significance level is calculated from the chi-square distribution, assuming the theoretical background red-noise spectrum, estimated using the lag one autocorrelation function (Gilman et al. 1963). The spectrum is smoothed by 5 points running average, giving to each point 10 degrees of freedom.

cycle removed (Fig. 5a) is dominated by the variability with the periods close to 15 days. This raw unsmoothed spectrum shows that there is a significant amount of variability present in all time scales. As will be discussed later, the variability at other time scales is also statistically significant (see Fig. 5b).

2) RELATIVE MAGNITUDE OF VARIABILITY OF OCEANIC HEAT TRANSPORT ON DIFFERENT TIME SCALES

To compare the variance of the heat transport on different time scales, we plot the standard deviations of the meridional heat transport over a range of period bands. These are shown in Fig. 6. Each time scale exhibits different variability with latitude. Overall, the time band with the largest amplitude is the seasonal cycle. Peak variability of the seasonal cycle occurs at 10°S and drops off rapidly south of the maximum but

more slowly into the NIO. Intraseasonal variability reaches the peak of 0.9 PW at the equator where it has a similar magnitude to the seasonal variability. The intraseasonal distribution is almost symmetrical about the equator indicating that this mode may be explained by equatorially trapped modes such as with Madden-Julian oscillations. The interannual signal is smallest in amplitude and more homogeneous in distribution. A relative maximum occurs near the equator from which it gradually decreases north and south. The standard deviation of the interannual variability of the cross-equatorial heat transport is about 0.1 PW, compared to a 1.2-PW yearly variation due to the seasonal cycle, or about one-tenth of the extreme of the heat transport seasonal cycle.

Figure 7 shows the standard deviations of different terms of the heat budget for the interannual variability. The variability of the heat transport is similar to the

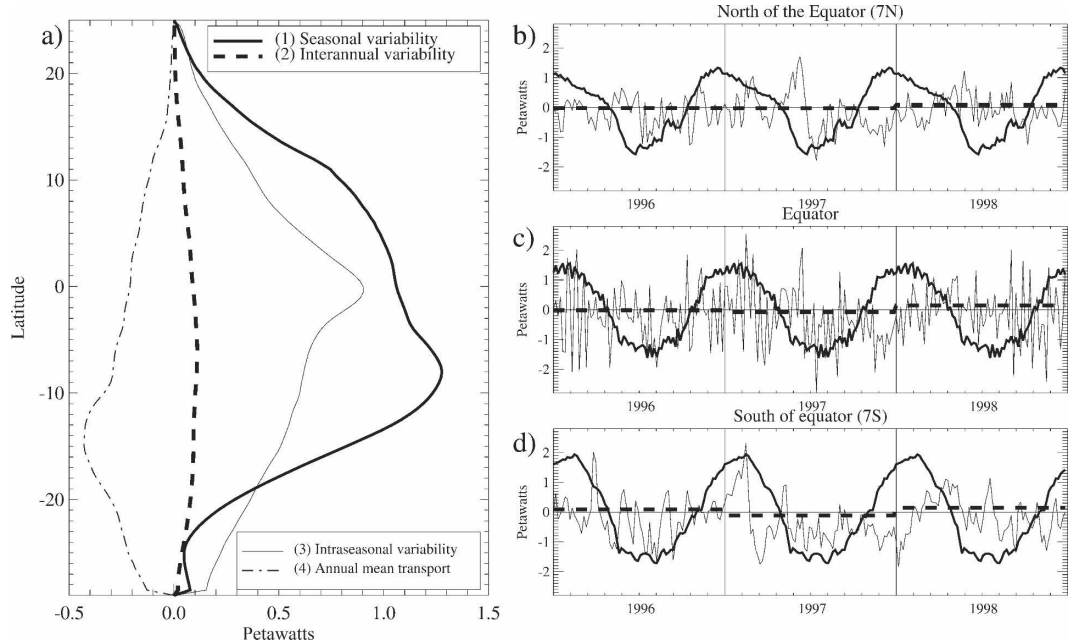


FIG. 6. (a) Amplitude of the variability of heat transport on different time scales as a function of latitude. The annual mean heat transport is plotted for reference. (Units: PW.) (b)–(d) Corresponding time series of the annual, seasonal, and intraseasonal variability at different latitudes for the years 1996–98. The long-term mean is subtracted from all time series.

variability of the rate of change of heat storage, and the variability of the surface heat flux is approximately half of the variability of the rate of change of heat storage. This holds up to 7°S, where the variability of the rate of change of the heat storage starts increasing sharply, and the heat transport variability starts decreasing. The results for the southern ocean are significantly affected by the absence of the ITF (see section 3e).

c. Interannual variability of the Indian Ocean heat transport

In the previous section, we obtained an estimate of the relative magnitude of variability of the Indian Ocean heat transport at different time scales. Now we will consider the annually averaged values and concentrate on the analysis of the interannual signal.

1) INTERANNUAL TIME SERIES OF THE NIO HEAT BALANCE

Figure 8a shows the annual averages of the cross-equatorial heat transport, the rate of change of heat storage in the NIO, and net surface flux into the NIO. Mean annual values of the cross-equatorial heat transport are generally negative. The predominantly negative values indicate that the southward summer transport is always bigger than the northward winter trans-

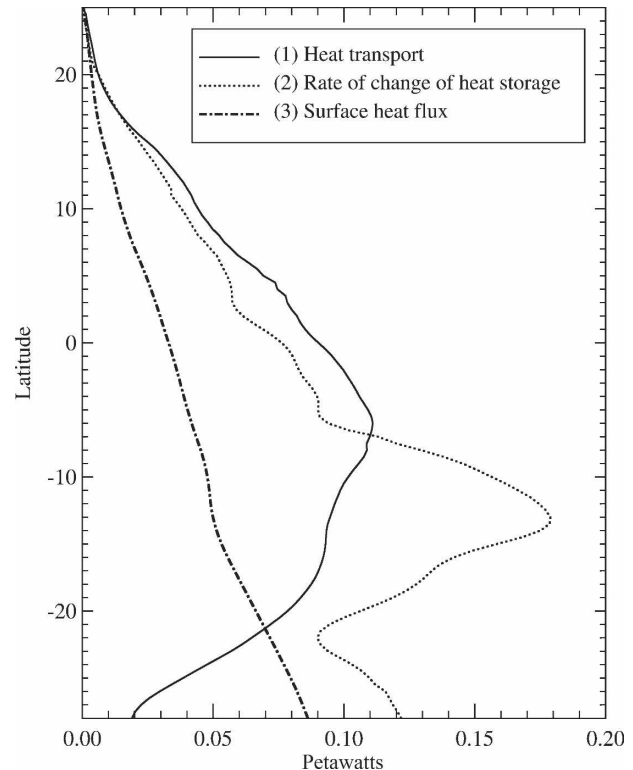


FIG. 7. Amplitude of the interannual variability of the heat transport, of the rate of change of heat storage, and of the net surface heat flux at the interannual time scales.

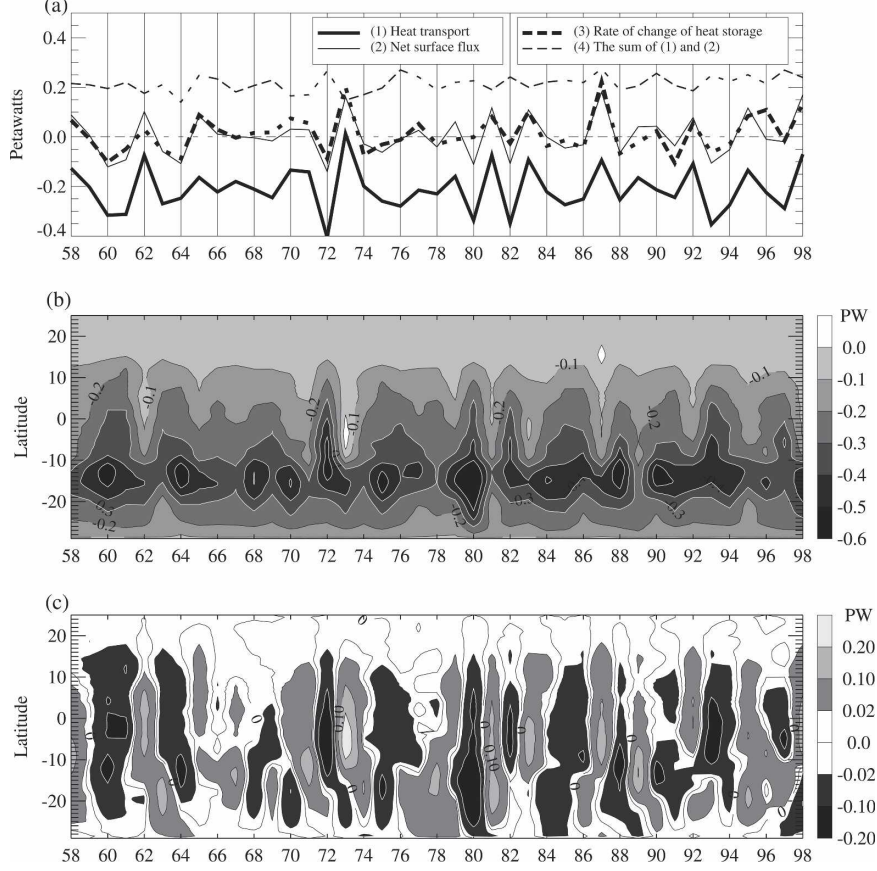


FIG. 8. (a) Annually averaged heat budget for the NIO. See legend for line definitions. (b) Space-time distribution of the annually averaged meridional heat transport (seasonal cycle is not removed). (c) Space-time distribution of the annually averaged anomalies of the meridional heat transport (seasonal cycle removed). Note the biennial tendency of the heat transport anomaly and that the anomalies have the same sign on the both sides of the equator, and extend laterally over most of the basin. (Units: PW.)

port, and therefore, on average the ocean dynamics acts to cool the NIO. There is considerable interannual variability in the magnitude of the cooling effect. Between 1958 and 1998 there are several years during which the deviation of the cross-equatorial heat transport from the mean values has the magnitude comparable to the mean values of the annual heat transport. For example, the annually averaged heat transport reaches a maximum negative value of -0.45 PW in 1972. In 1973 the heat transport is slightly positive and exceeds the mean by $+0.2$ PW. This is the only year out of 41 yr, when the annually averaged heat transport has positive sign, which is the opposite sign compared to the long-term negative mean value. The deviation from the long-term mean in the years 1972 and 1973 is about one-tenth of the amplitude of the seasonal cycle.

Given the degree of interannual variability in the cross-equatorial heat transport noted in Fig. 8, it is rea-

sonable to ask whether it is related to other interannual signals such as ENSO. However, the correlation coefficient between the annually averaged cross-equatorial heat transport and the Niño-3 SST¹ is only -0.1 suggesting a weak or nonsignificant relationship. As the amplitude of the SST anomaly associated with El Niño peaks in the November–March period, we calculate the lagged correlation of the November–March Niño-3 index with the total heat transport. It turns out that the correlation of the winter Niño-3 with the following year heat transport is 0.32 , which is significant at 90% indicating, perhaps, that the Pacific Ocean is one of the components involved in the heat balance of the Indian Ocean. By comparing the annual means of the heat

¹ Niño-3.4 is the SST anomaly averaged over 5°S , 5°N and 120° , 170°W .

transport with winter Niño-3.4 index, we can see that in many cases the El Niño years correspond to the cross-equatorial heat transport anomalies switching from negative (anomalously southward transport) to positive (anomalously north transport). This is true for the years 1972–73, 1982–83, 1986–87, and 1997–98. In several cases the enhanced southward transport corresponds to strong monsoon years (1975, 1988, 1994), and enhanced northward transport to the weak monsoon years (1965, 1979, 1987), where strong and weak monsoon years are defined by the All India Rainfall Index (AIRI; Parthasarathy et al. 1994). However, over the totality of the 41-yr time period, the correlation between AIRI (which is calculated for the summer months from June to September), and the total heat transport is essentially zero, as is the correlation between AIRI and summer heat transport, indicating that there is no linear relationship between these variables. Anomalies in the mean annual heat transport result from anomalous heat transport at all times of the year. As could be seen from Fig. 4, the variability does not have any preferred season. For example, from Fig. 8a we can see that in 1987 there is strong northward annual heat transport anomaly, and in 1988 there is noticeable southward annual heat transport anomaly. From Fig. 4 it appears that in 1987 the annual anomaly results from the strong positive anomaly is spring, while in 1988, the spring is almost average although large anomalies occur during the rest of the year.

Figure 8a appears to possess a biennial tendency of the heat transport variability in the sense that a year with strong southward anomaly is often followed by a year with strong northward anomaly and vice versa. To obtain a more quantitative description of the time series, the every 5-day model output was filtered by running a convolution with a digital filter. The filter leaves unchanged all frequencies higher than 0.9 yr^{-1} , reducing frequencies to zero as a cosine function. That is, the filter removes efficiently variability with frequencies higher than one year. Figure 5b shows the spectrum of the filtered 5-day time series. Only the part of the spectrum corresponding to the period larger than one year is plotted. To be more confident about the significance of the individual peaks, a 5-point running average is applied to the spectrum. The dashed line indicates the 99% significance level relative to the background spectrum shown by thin solid line. The significance level is calculated from the chi-square distribution, assuming theoretical background red-noise spectrum, and is estimated using lag one autocorrelation function (Gilman et al. 1963). Two significant peaks centered around 2.1 yr and around 1.3 yr are now evident. The peak at 2.1 yr indicates the presence of the broadband biennial

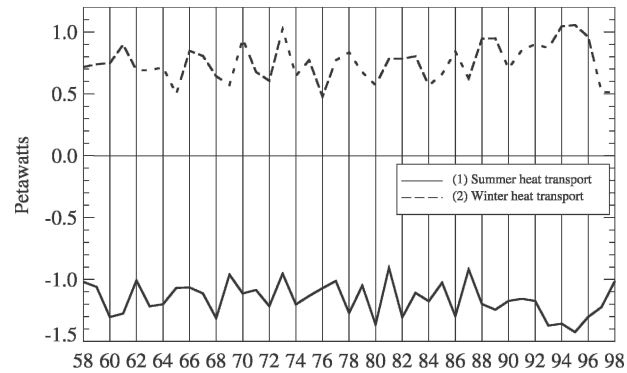


FIG. 9. Time series of the winter and summer heat transport. Each point is the average of the corresponding summer (May–October) or next winter (November–April) heat transport. The values of the winter transport correspond to the next season relative to the time axis, i.e., the value for the year 1958 corresponds to the winter of 1958/59.

component, confirming the peak we had noted visually in Fig. 8a.

2) COMPARISON OF SUMMER AND WINTER HEAT TRANSPORT

In an attempt to investigate further the seasonal structure of the mean annual heat transport, it is separated into winter and summer periods. For the purpose of the analysis, the definition of winter and summer periods is based on the time of the year when the mean seasonal cycle of the Indian Ocean heat transport changes sign as apparent in Figs. 1 and 3. Figure 9 presents the time series of the cross-equatorial heat transport for winter (November through April: upper line) and summer (May through October: lower line) months. The correlation between summer and next winter transport is -0.30 . Lagged by a half a year, the correlation between summer and previous winter transport is -0.45 , again suggesting a biennial character to the heat transport variability, consistent with the conclusion of Meehl (1987) and Yasunari (1991). In our case both correlations (i.e., summer with previous winter and winter with previous summer) are negative, which mean that if the winter heat transport is anomalously positive, then the next summer heat transport is anomalously negative and so on. These relationships suggest that if there are strong winds during the winter (anomalously strong northward Ekman transport) then there will be strong winds during summer (anomalously strong southward Ekman transport).

3) LATITUDINAL DISTRIBUTION OF ANNUALLY AVERAGED MERIDIONAL HEAT TRANSPORT

In section 3b(1) we noticed that the interannual variability is relatively homogeneous in latitude in contrast

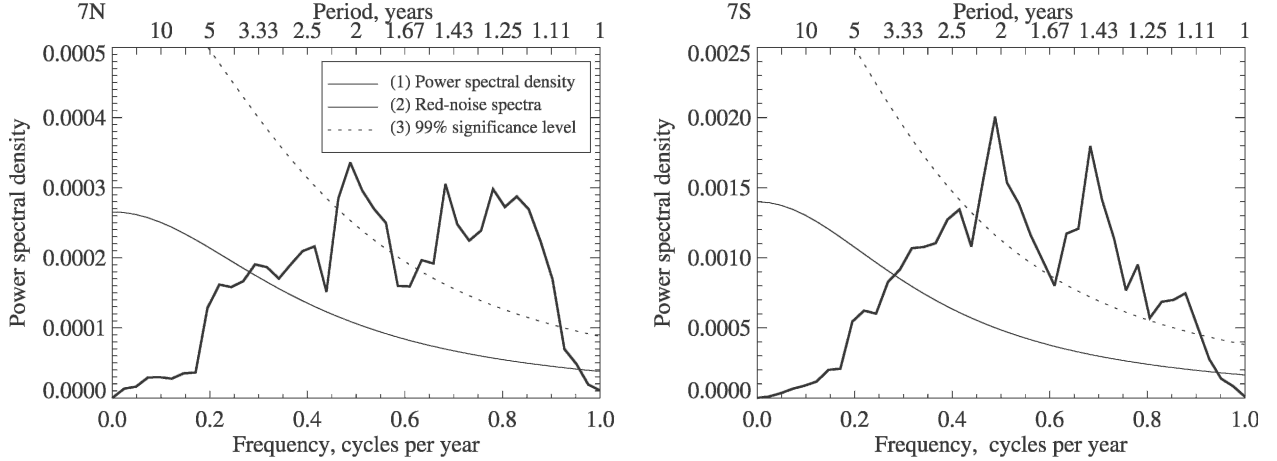


FIG. 10. Power spectrum of the cross-equatorial heat transport at (left) 7°N and (right) 7°S. The part of the spectrum corresponding to frequencies larger than one year is shown. The seasonal cycle is removed by excluding the first four annual harmonics. The spectrum is smoothed, and the significance level is plotted in the same way as in Fig. 5.

to the intraseasonal and seasonal variability. The latitudinal distribution of the annually averaged heat transport is presented in Fig. 8b. Maximum southward transport up to -0.8 PW occurs between 5°S and 20°S. This is the same feature as was observed for the mean seasonal cycle, shown in Fig. 1.

A comparison of Figs. 8a,b, suggests that either anomalously strong or weak meridional heat transport occurs at all latitudes during a particular year. That is, if the transport is anomalously southward at the equator it is anomalously southward at all latitudes. For example, in 1980 there is universally strong transport at all latitudes, whereas in 1981 it is weak at all latitudes. This latitudinal commonality of the sign of the anomalous transports is emphasized in Fig. 8c where the long-term annual average mean heat transport is removed. In general, same signed anomalies in the meridional heat transport extend from the northern to southern limits of the basin and, as such, show the same sign on either side of the equator. Jayne and Marotzke (2001) found similar pattern for the World Ocean heat transport, that is, that the interannual variations of the heat transport are coherent over large meridional extents.

Figure 10 shows the power spectrum of the heat transport calculated at 7°N and 7°S. The comparison of Fig. 10 with Fig. 5 shows that the strong broadband biennial signal is present across the central part of the ocean. The cross-equatorial extension of same-signed anomalies suggest that, in contrast to the mean seasonal cycle, the processes that produce the interannual variability of the heat transport are relatively homogeneous across the ocean basin. To test this hypothesis we considered the part of the basin north of 10°S and south of 15°N; 10°S is the latitude of the most rapid SST change.

North of this latitude the Indian Ocean is mostly affected by changing monsoon winds, while south of this latitude there are southeasterlies at all times of the year. A northern limit 15°N is chosen to smooth the effects of the rather complicated basin shape in the NIO. We call a year positive if the heat transport anomaly for that year between 10°S–15°N is always positive, and reaches at least +0.1 PW. We call a year negative if the heat transport anomaly in the band is always negative, and reaches at least -0.1 PW. Using these criteria, nine positive and nine negative years were found out of the total of 41 yr. Figure 11 shows the resulting composite heat transport anomalies for positive (Fig. 11a) and negative (Fig. 11b) years. It is apparent that the annually averaged anomalies result from heat transport being anomalously positive or negative at all times of the year. The amplitude of the anomalies for positive and negative years is very similar. For positive years the largest values are +0.8 PW, while for negative years the values reach -1.0 PW. The standard deviation for both negative and positive years is 0.15 PW and is largest at the equator in both cases (0.32 and 0.26 PW for positive and negative years, respectively) falling off rapidly away from the equator. In addition, the activity of the intraseasonal variability appears stronger in negative years. Interestingly, the anomaly patterns for positive and negative years are strongly correlated with a coefficient of -0.42 . Stronger correlations are observed near the equator and around 10°N and 10°S. Figure 11c shows the correlation between composite time series for positive and negative years for all latitudes. The strongest correlation of -0.54 is observed at 2.5°N, and decreases rapidly toward north and south.

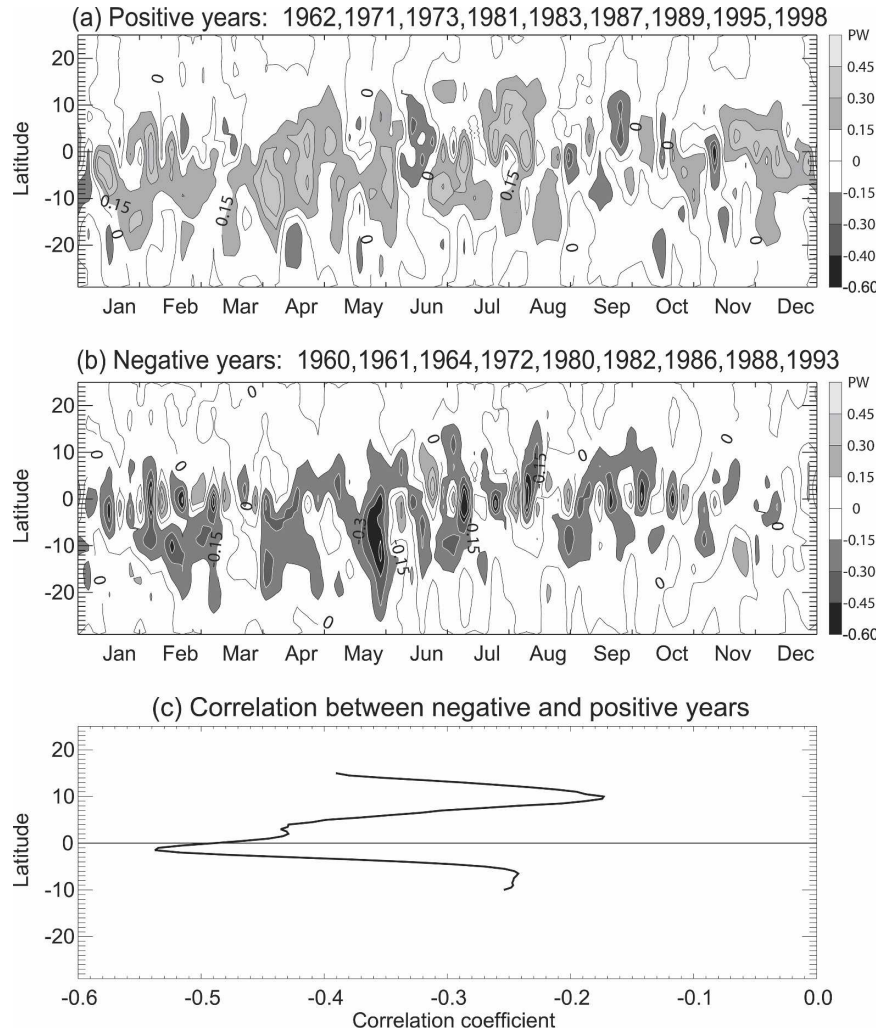


FIG. 11. Composite seasonal cycle of the anomalous heat transport for the years during which the annually averaged heat transport anomalies have the same sign [(a) positive and (b) negative] across the central part of the ocean. Changes for the negative and positive years appear to be almost opposite to each other. (c) Correlation of the time series from (a) and (b) as a function of latitude.

d. Ekman contribution to the meridional heat transport

Jayne and Marotzke (2001) and Miyama et al. (2003), as well as a number of other studies, suggest that most of the heat transport variability results from the Ekman transport. Following Levitus (1987), the oceanic Ekman heat transport could be estimated as

$$Q_v(\text{EK}) = \rho c_p \int \frac{-\tau^{(x)}}{f} [T_s - (T)] dx, \quad (7)$$

where T_s is the sea surface temperature, (T) is the vertically averaged temperature (or a deep reference temperature), $\tau^{(x)}$ is the zonal wind stress, and f is the Coriolis parameter. Figure 12 shows the annually averaged Ekman transport and meridional heat transport as a function of latitude for the years 1968, 1973, and 1987. Since the Ekman transport is not defined at the equator, there is corresponding discontinuity. These years were chosen to show that in the equatorial region the relationship between the heat transport and the Ekman transport varies a lot from one year to another. For the years 1973 and 1987 there is much more similarity between two curves, while for the year 1968 two curves are very different for most part of the ocean. To improve the estimation of this variability, we calculate the correlation between the Ekman transport and heat transport for two different time scales: one calculation

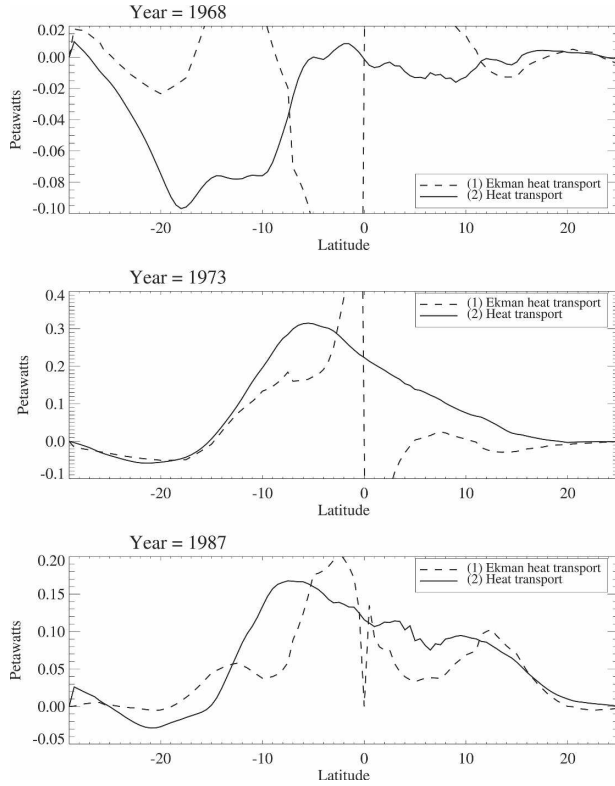


FIG. 12. Annually averaged meridional heat transport and Ekman heat transport as a function of latitude for the years: (top) 1968, (middle) 1973, and (bottom) 1987. The relationship between the Ekman heat transport and the heat transport changes strongly from one year to another.

uses annually averaged values of the Ekman transport and heat transport, and another uses time series from the model output at every 5 days.

Figure 13 shows the time series of the heat transport and Ekman transport at 5-day intervals for the years 1981 and 1982. The time series correspond to the meridional heat transport across 7°N (Fig. 13a) and 7°S (Fig. 13b). The 7°N and 7°S were chosen because these latitudes are not strongly affected by the ITF in the southern part of the ocean, and not strongly affected by the northern boundary in the northern Indian Ocean. At the same time, the latitudes within 5° of the equator are affected by the discontinuity in the Ekman transport. Figure 13c shows the correlation between the annually averaged values of the Ekman transport and the annually averaged values of the heat transport, calculated from 41-yr time series with 5-day model output. The correlation is calculated as a function of latitude. We can see that the correlation is above 0.8 for most parts of the ocean. The two exceptions are near the equator, where the concept of the Ekman transport is not valid, and in the northernmost part of the ocean,

where the heat transport is probably strongly affected by the presence of land. Figure 14 shows the annually averaged meridional heat transport and Ekman transport at 7°N (Fig. 14a) and 7°S (Fig. 14b), and corresponding correlation between the time series of the annually averaged Ekman transport and heat transport. For most part of the basin the correlation is above 0.4, which is significant at 90%. The worst correlation is between the equator and 10°N .

Jayne and Marotzke (2001) suggested the dynamical explanation of the heat transport variability. The important part of their explanation is the difference between mechanisms driving the time-mean and time-varying parts of the Ekman transport. They demonstrate that for the time-mean Ekman transport the resulting compensating flow is highly baroclinic, however, for the time-varying part of the Ekman transport the compensating return flow is barotropic; that is, depth-independent, extending to the full depth of the ocean. The two-and-a-half-layer model used in this study does not have a barotropic mode. Figure 14 shows a time series for the years 1981 and 1982 indicating a strong correlation between the Ekman transport and the heat transport. Such a good correlation suggests that the barotropic return flow is not required to explain the heat transport variability at short time scales.

e. Influence of the Indonesian Throughflow

As mentioned earlier, the model used in the current study does not take into account the ITF. As has been pointed by many authors (Hirst and Godfrey 1993; Godfrey 1996; Webster et al. 1998; Vranes et al. 2002; Wajsowicz and Schopf 2001) the ITF is considered central to the heat budgets of the Pacific and Indian Oceans. However, there is considerable uncertainty in the mean ITF transport and its variability. Vranes et al. (2002) for example, provide estimates of mean ITF mass transport from a number of studies that range from near zero to 30 Sv, with an interannual component of between ± 5 Sv with larger transports with La Niña, and smaller transports with El Niño.

Several papers have considered the impact of the ITF on the Indian Ocean heat transport. All studies are consistent in that the addition of the ITF produces stronger currents and stronger temperature gradients along 10°S . McCreary et al. (1993) show that in the model used in our current study the ITF produces similar effect in the Southern Hemisphere. However, according to Schott and McCreary (2001) and Vranes et al. (2002) the pathways of the ITF water within the Indian Ocean are still very much a matter of debate. Wajsowicz and Schopf (2001) show that this stronger

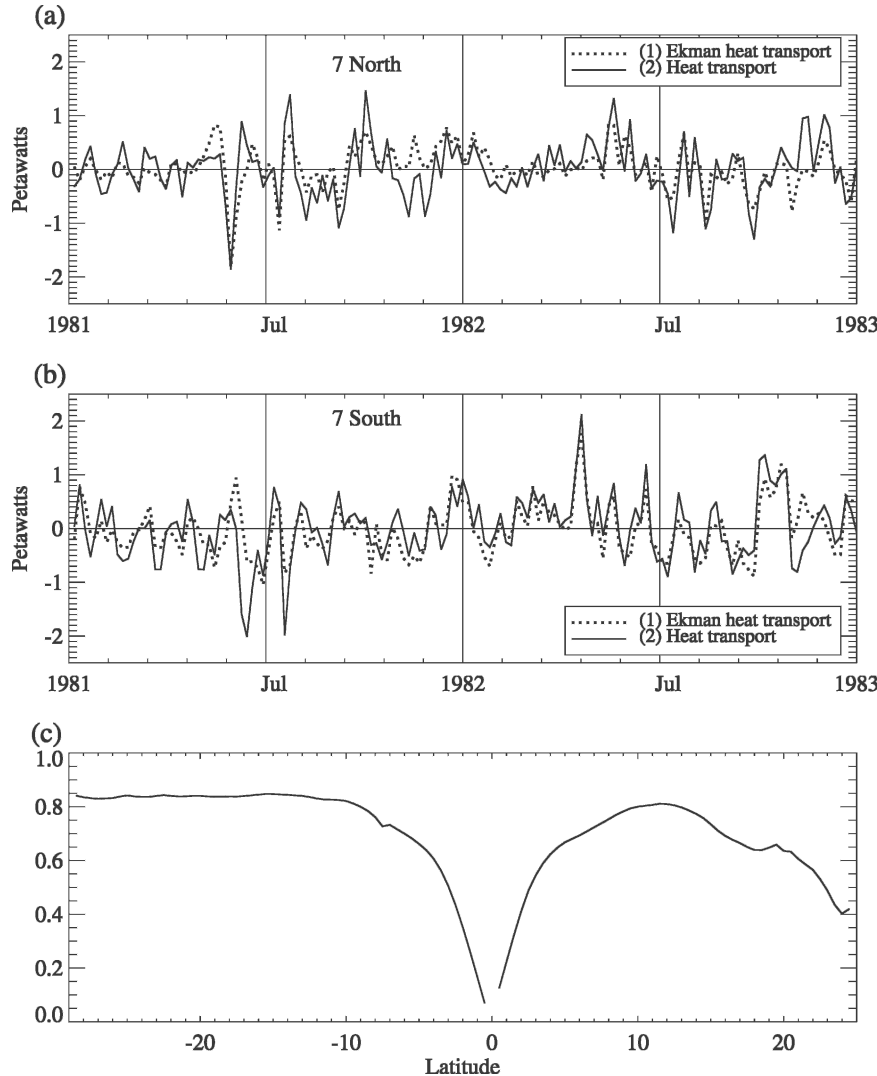


FIG. 13. Anomaly time series of the Ekman heat transport and heat transport for the years 1982–83 at (a) 7°N and (b) 7°S. The anomaly time series are obtained by subtracting the corresponding annual means. (c) The correlation between the anomalies of the Ekman heat transport and heat transport as a function of latitude. Correlation is calculated from the time series for 41 yr with 5-day sampling.

currents lead to the suppression of the southward meridional transport from Arabian Sea to the southern Indian Ocean during boreal summer, and makes SSTs in the Arabian Sea higher. Vranes et al. (2002) found that the heat flux divergence of the ITF waters within the Indian Ocean north of 30°S is not significant, and that the ITF heat is ultimately lost to the atmosphere in the southwest Indian Ocean. Ferron and Marotzke (2003), on the other hand, find that the heat transport north of the ITF in the upper 1000 m of the ocean does not depend on the ITF. Thus, there is still uncertainty in the impact of the ITF on the heat budget of the Indian Ocean.

We conducted two experiments to investigate how the ITF would affect our results. Following Han (1999) and McCreary et al. (1993), we added the ITF to the model. The ITF was added by replacing the closed boundary conditions on u_i and T_i at the eastern boundary segment, $x = 115^\circ\text{E}$ and $9^\circ\text{S} \leq y \leq 16^\circ\text{S}$. The new boundary conditions are

$$u_i = -V_i/(h_i L_f), \quad T_i = T_i^*, \quad (8)$$

where $V_1 = 7 \text{ Sv}$, $V_2 = 3 \text{ Sv}$, $T_1 = 28^\circ\text{C}$, $T_2 = 16^\circ\text{C}$, and $L_f = 7^\circ$ is the throughflow area. The above values are suggested by observations or previous modeling studies. We refer to the model run with the ITF included as

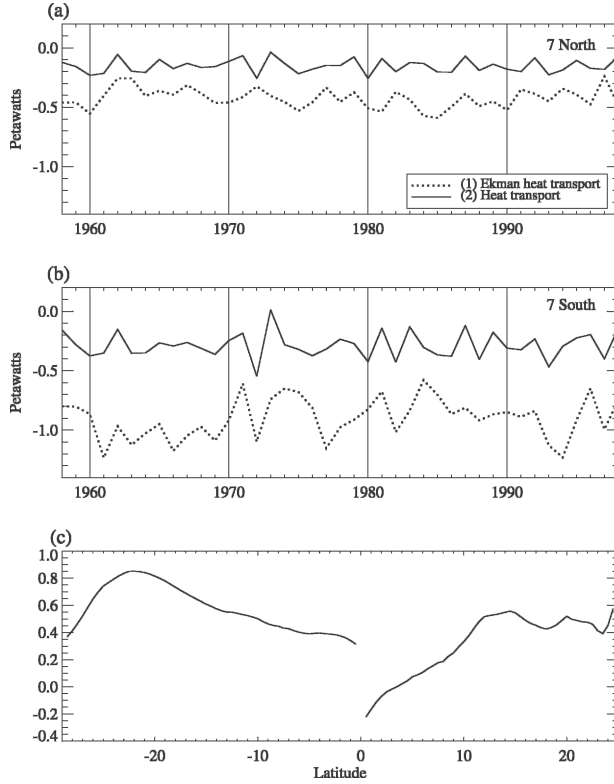


FIG. 14. Time series of the annually averaged Ekman heat transport and heat transport for the years 1982–83 at (a) 7°N and (b) 7°S. (c) The correlation between the anomalies of the Ekman heat transport and heat transport as a function of latitude. Correlation is calculated from the time series consisting of 41 annually averaged values.

the ITF run, and the model run without the ITF as the main run.

To estimate the influence of the ITF we calculate the difference between the ITF run and the main run. Fig-

ure 15 shows the difference in the mean annual currents. The main impact of the ITF is the strong current across the ocean around 10°S. These results are remarkably similar to the corresponding difference fields in the global GCM solution of Hirst and Godfrey (1993). Figure 16 shows the heat transport difference between the ITF run and the main run. The most noticeable changes occur to the south of 10°S, where a substantial decrease in northward heat transport is seen. This is the consequence of the ITF water being warmer than the Indian Ocean water. In the region between equator and 10°S there is a small northward heat transport decrease in spring (March–May), and a small northward heat transport increase in winter (November and December). All differences occurring north of 10°S do not exceed 0.2 PW, which is an order of magnitude smaller than the annual cycle of the heat transport. In the southern part of the ocean the biggest difference occurs in April and May, reaching the maximum values of −0.8 PW. When adding the ITF to the model we assumed that there is no seasonal variation in the ITF strength. The annual variation of the ITF results in the ITF being strongest in August, and weakest in February. This annual cycle may result in even smaller differences in the annual cycle of the heat transport. The maximum northward transport decrease is seen in April–May, and February is the time of the minimum ITF transport; therefore, the seasonal variation will make the ITF effect smaller during winter, making the annual cycle of the heat transport more similar to the case without the ITF. This suggests that the ITF does not significantly alter the Indian Ocean heat transport in the part of the ocean north of 10°S.

To estimate the effect of the ITF on the interannual variability of the heat transport, we made model runs with the interannual variability of the ITF. As of today,

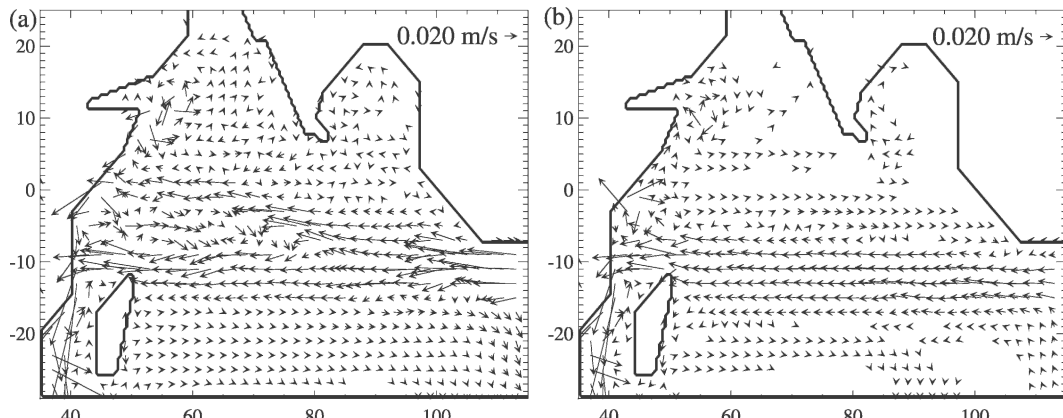


FIG. 15. Annually averaged currents by lat-lon, ITF run minus main run for the (left) upper layer and (right) lower layer. The main impact of the ITF is the strong current across the ocean around 10°S.

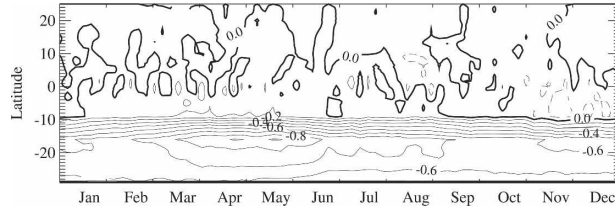


FIG. 16. Annual cycle of the heat transport. ITF run minus main run. The most noticeable changes occur to the south of 10°S , where a substantial decrease in the northward heat transport is seen.

there is no long-term observational data for the ITF transport variability. However, several studies suggest that the ITF transport changes with the phase of the ENSO by as much as $\pm 5 \text{ Sv}$, with smaller transport during El Niño, and bigger transport during La Niña

(see Vranes et al. 2002, and references therein). We constructed the interannual variability of the ITF, making the ITF to vary according to ENSO phase. We took the mean ITF equal to 10 Sv , which agrees with observations. Warm and cold episodes were defined by the threshold $\pm 0.5^{\circ}\text{C}$ for the Oceanic Niño Index (ONI) 3-month running mean of ERSST.v2 SST (Smith and Reynolds 2004) anomalies in the Niño-3.4 region based on the 1971–2000 base period. We scaled the monthly ITF transport according to the ENSO phase and strength, and then found the mean ITF transport for each year. Then we ran the model with the ITF varying according to this artificial cycle. Figure 17 shows the resulting difference in the interannual variability of the heat transport as the difference between the variable ITF run and the main run. As could be seen from Fig. 17a the equatorial annually averaged values of the heat

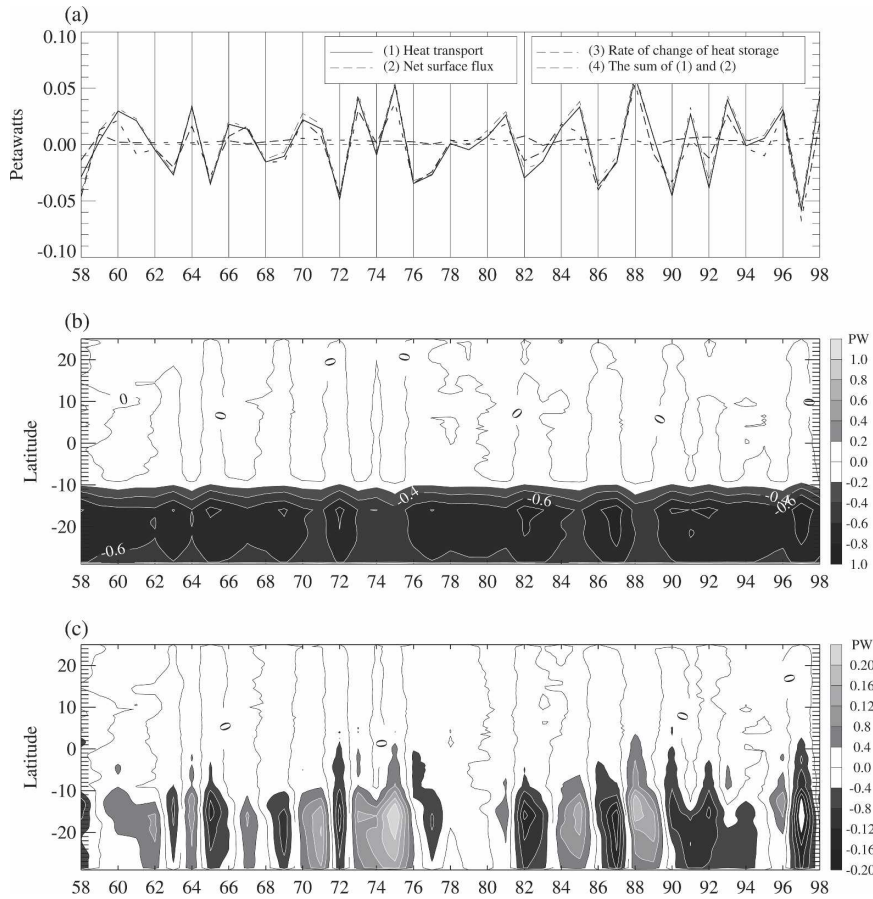


FIG. 17. Time series of the annually averaged heat transport for the ITF run minus main run. (a) Annual means of the heat balance of the NIO (ITF run – main run). The equatorial annually averaged values of the heat transport could change by as much as $\pm 0.5 \text{ PW}$ as a result of the addition of the ITF. (b) Annually averaged meridional oceanic heat transport. The enhanced southward transport occurs in the southern Indian Ocean, to the south of 10°S . (c) Anomalies of the annually averaged meridional oceanic heat transport (ITF run – main run).

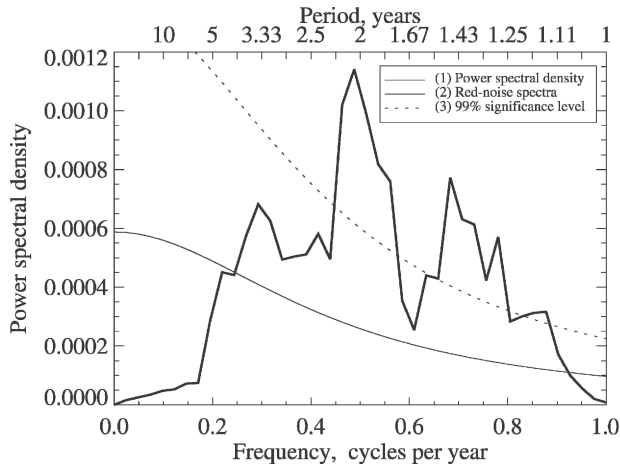


FIG. 18. Power spectrum of the cross-equatorial heat transport for the ITF run. The part of the spectrum corresponding to frequencies larger than one year is shown. The seasonal cycle is removed by excluding the first four annual harmonics. The spectrum is smoothed, and the significance level is plotted in the same way as in Fig. 5.

transport could change by as much as ± 0.5 PW as a result of the addition of the ITF. Figure 17b shows that the addition of the ITF produces an additional band of negative heat transport, which corresponds to the enhanced southward transport. The enhanced southward transport occurs in the southern Indian Ocean, to the south of 10°S . Figure 17c shows the difference of the heat transport anomalies between the variable ITF run and the main run. The change of the heat transport anomalies due to the inclusion of the ITF is as big as the interannual anomalies of the heat transport variability in the southernmost part of the ocean. We note that for some years the difference is seen in the entire ocean south of the equator; this is especially noticeable for the years 1972, 1988, 1997. Figure 18 shows the power spectrum of the equatorial time series with the addition of the ITF, showing that the main frequencies of the interannual variability are not affected by the inclusion of the ITF, in particular the biennial frequency.

4. Conclusions

The interannual variability of the Indian Ocean meridional heat transport was investigated using the 41-yr time series produced by a two-and-a-half-layer reduced gravity ocean model, forced by the NCEP–NCAR reanalysis product. It was found that the oceanic heat transport exhibits strong variability at all time scales from intraseasonal to interannual; that is, from 10 days to several years. On intraseasonal time scales (10–90

days) the net surface flux, the oceanic heat transport, and the rate of change of the heat storage undergo quick and high-amplitude variations, comparable to the amplitude of the mean seasonal cycle. This variability is consistent with the findings of Jayne and Marotzke (2001), who determined that the short-term heat transport fluctuations near the equator could completely compensate the seasonal signal. However, this finding may be contrary to Behera et al. (2000) who concluded that the warming of some regions in the southern tropical Indian Ocean is explained primarily by the variability of surface latent heat flux and entrainment. The variability of the heat transport and change of the heat storage is much bigger than the variability of the net surface flux (e.g., Figs. 4,7), which suggests that internal ocean dynamics are actively involved in the redistribution of heat.

A broadband biennial signal was detected in the meridional heat transport. This result is consistent with Meehl (1997), who found that the quasi-biennial signal could arise from switching from strong to weak monsoon, occurring sometimes every year, and sometimes every two years, which will produce a broadband peak around 2 yr in the Fourier spectrum. One of the limitations of the model used for this study is the absence of the ITF. The test runs with the ITF included show that the ITF mostly affects the part of the ocean south of 10°S . The comparison of Figs. 5 and 18 shows that the major frequencies of the interannual variability of the northern part of the ocean, including the broadband biennial signal, are not affected by the presence of the ITF.

On interannual time scales the meridional heat transport often changes simultaneously at all latitudes. This finding is consistent with Jayne and Marotzke (2001) who found that interannual variations of the heat transport are coherent over large meridional extents for the World Ocean. The biennial signal is present across the central part of the Indian Ocean. The correlation patterns obtained for the years of the homogeneous negative or positive meridional heat transport across the whole Indian Ocean suggest that there are some broad-scale mechanisms that govern the heat transport anomalies in the opposite ways for positive and negative years. Loschnigg and Webster (2000) and Webster et al. (2002b) found similar patterns of interannual variability of the Indian Ocean heat transport. We found that the heat transport and Ekman transport are highly correlated over much of the ocean. At 0.8, the correlation is especially high in the 5-day time series suggesting that heat transport anomalies could be explained by the Ekman transport anomalies on intraseasonal time

scales, and partially explained by the Ekman transport anomalies on the interannual time scales.

Ekman theory, however, is not valid at the equator where we found the highest correlation between the years with negative and positive heat transport anomalies. Two different theories have been suggested recently for the cross-equatorial flow. Both theories take into account that the annual-mean component of the zonal wind stress is predominantly antisymmetric about the equator. Miyama et al. (2003) suggested that the surface cross-equatorial flow is driven by the annual-mean component of the zonal wind stress. Jayne and Marotzke (2001) argued that the Ekman transport does not need to be defined at the equator because as the Coriolis force vanishes there, the flow is carried across the equator by continuity and direct pressure gradient forcing. Both theories agree that the cross-equatorial heat transport will be close to Ekman transport on both sides of the equator. However, Jayne and Marotzke (2001) also point out, that the poorest agreement is in the tropical Indian Ocean. The possible reason for that could be that the strong meridional winds there tend to suppress the heat transport (Bryan 1982).

The current study has demonstrated the importance of intraseasonal and interannual variability of the meridional heat transport in the Indian Ocean, and outlined main patterns of the temporal and spatial variability of the heat transport. Further investigation of the intraseasonal variability of the heat transport is needed to gain a better insight into the mechanisms affecting the variability.

Acknowledgments. This work has been supported by National Science Foundation under Grant ATM-0120956. Thanks to Prof. J. P. McCreary for the generously supplied initial ocean model code, and Prof. Weiqing Han and Dr. J. Loschnigg for many interesting discussions. We also appreciate the comments of the anonymous reviewers.

REFERENCES

- Anderson, D., 1999: Extremes in the Indian Ocean. *Nature*, **401**, 337–339.
- Behera, S. K., P. S. Salvekar, and T. Yamagata, 2000: Simulation of interannual SST variability in the tropical Indian Ocean. *J. Climate*, **13**, 3487–3499.
- Bhat, G. S., and Coauthors, 2001: BOBMEX—The Bay of Bengal Monsoon Experiment. *Bull. Amer. Meteor. Soc.*, **82**, 2217–2245.
- Bryan, K., 1982: Seasonal variation in meridional overturning and poleward heat transport in the Atlantic and Pacific Oceans: A model study. *J. Mar. Res.*, **40** (Suppl.), 39–53.
- Clarke, A. J., X. Liu, and S. V. Gorder, 1998: Dynamics of the biennial oscillation in the equatorial Indian and far western Pacific oceans. *J. Climate*, **11**, 987–1001.
- Darnell, W. L., W. F. Staylor, N. A. Ritchey, S. K. Gupta, and A. C. Wilber, 1996: Surface radiation budget: A long-term global dataset of shortwave and longwave fluxes. [Eos Electronic Supplement, available online at http://www.agu.org/eos_elec/95206c.html.]
- Feng, M., and G. Meyers, 2003: Interannual variability in the tropical Indian Ocean: A two-year time-scale of Indian Ocean Dipole. *Deep-Sea Res.*, **50**, 2263–2284.
- Ferron, B., and J. Marotzke, 2003: Impact of 4d-variational assimilation of WOCE hydrography on the meridional circulation of the Indian Ocean. *Deep-Sea Res.*, **50**, 2005–2021.
- Fu, L., 1986: Mass, heat and freshwater fluxes in the South Indian Ocean. *J. Phys. Oceanogr.*, **16**, 1683–1693.
- Garternicht, U., and F. Schott, 1997: Heat fluxes of the Indian Ocean from a global eddy-resolving model. *J. Geophys. Res.*, **102**, 21 147–21 159.
- Gilman, D. L., F. J. Fuglister, and J. M. Mitchell Jr., 1963: On the power spectrum of “red noise.” *J. Atmos. Sci.*, **20**, 182–184.
- Godfrey, J. S., 1996: The effect of the Indonesian throughflow on ocean circulation and heat exchange with the atmosphere: A review. *J. Geophys. Res.*, **101**, 12 217–12 237.
- Goswami, B. N., 1995: A multiscale interaction model for the origin of the tropospheric QBO. *J. Climate*, **8**, 524–534.
- Hall, M. M., and H. L. Bryden, 1982: Direct estimates and mechanisms of ocean heat transport. *Deep-Sea Res.*, **29**, 339–359.
- Han, W., 1999: Influence of salinity on dynamics, thermodynamics, and mixed-layer physics in the Indian Ocean. Ph.D. dissertation, Nova Southeastern University, 147 pp.
- Han, W. Q., and P. J. Webster, 2002: Forcing mechanisms of sea level interannual variability in the Bay of Bengal. *J. Phys. Oceanogr.*, **32**, 216–239.
- , D. M. Lawrence, and P. J. Webster, 2001: Dynamical response of equatorial Indian Ocean to intraseasonal winds: Zonal flow. *Geophys. Res. Lett.*, **28**, 4215–4218.
- Hastenrath, S., and P. J. Lamb, 1980: On the heat budget of the hydrosphere and atmosphere in the Indian Ocean sector. *J. Phys. Oceanogr.*, **10**, 694–708.
- , and L. Greischar, 1993: The monsoonal heat budget of the hydrosphere-atmosphere system in the Indian Ocean sector. *J. Geophys. Res.*, **98**, 6869–6881.
- Hirst, A. C., and J. S. Godfrey, 1993: The role of Indonesian Throughflow in a global ocean GCM. *J. Phys. Oceanogr.*, **23**, 1057–1086.
- Hsiung, J., R. E. Newell, and T. Houghtby, 1989: The annual cycle of oceanic heat storage and oceanic meridional heat transport. *Quart. J. Roy. Meteor. Soc.*, **115**, 1–28.
- Huang, B., and J. L. Kinter III, 2002: Interannual variability in the tropical Indian Ocean. *J. Geophys. Res.*, **107**, 3199, doi: 10.1029/2001JC001278.
- Jayne, S. J., and J. Marotzke, 2001: The dynamics of ocean heat transport variability. *Rev. Geophys.*, **39**, 385–411.
- Kalnay, E., and Coauthors, 1996: The NCEP/NCAR 40-Year Reanalysis Project. *Bull. Amer. Meteor. Soc.*, **77**, 437–471.
- Kistler, R., and Coauthors, 2001: The NCEP-NCAR 50-Year Reanalysis: Monthly means CD-ROM and documentation. *Bull. Amer. Meteor. Soc.*, **82**, 247–268.
- Kraus, E. B., and J. S. Turner, 1967: A one-dimensional model of the seasonal thermocline II: The general theory and its consequences. *Tellus*, **19**, 98–106.
- Lee, T., and J. Marotzke, 1997: Inferring meridional mass and heat transports of the Indian Ocean by fitting a general cir-

- culation model to climatological data. *J. Geophys. Res.*, **102**, 10 585–10 602.
- , and —, 1998: Seasonal cycles of meridional overturning and heat transport of the Indian Ocean. *J. Phys. Oceanogr.*, **28**, 923–943.
- Levitus, S., 1982: *Climatological Atlas of the World Ocean*. NOAA Professional Paper 13, 163 pp + 17 microfiches.
- , 1987: Meridional Ekman heat fluxes for the World Ocean and individual ocean basins. *J. Phys. Oceanogr.*, **17**, 1484–1492.
- Loschnigg, J. P., and P. J. Webster, 2000: A coupled ocean-atmosphere system of SST modulation for the Indian Ocean. *J. Climate*, **13**, 3342–3360.
- , G. A. Meehl, P. J. Webster, J. M. Arblaster, and G. P. Compo, 2003: The Asian monsoon, the tropospheric biennial oscillation, and the Indian Ocean zonal mode in the NCAR CSM. *J. Climate*, **16**, 1617–1642.
- McCreary, J. P., Jr., P. K. Kundu, and R. L. Molinari, 1993: A numerical investigation of dynamics, thermodynamics, and mixed-layer processes in the Indian Ocean. *Progress in Oceanography*, Vol. 31, Elsevier, 181–244.
- Meehl, G. A., 1987: The annual cycle and interannual variability in the tropical Pacific and Indian Ocean regions. *Mon. Wea. Rev.*, **115**, 27–50.
- , 1997: The South Asian monsoon and the tropospheric biennial oscillation. *J. Climate*, **10**, 1921–1943.
- Miyama, T., J. P. McCreary Jr., T. G. Jensen, J. Loschnigg, S. Godfrey, and A. Ishida, 2003: Structure and dynamics of the Indian Ocean cross-equatorial cell. *Deep-Sea Res.*, **50**, 2032–2047.
- Murtugudde, R., and A. J. Busalacchi, 1999: Interannual variability of the dynamics and thermodynamics of the tropical Indian Ocean. *J. Climate*, **12**, 2300–2326.
- Nicholson, S. E., and B. S. Nyenzi, 1990: Temporal and spatial variability of SSTs in the tropical Atlantic and Indian Oceans. *Meteor. Atmos. Phys.*, **42**, 1–17.
- Oberhuber, J. M., 1988: An atlas based on the COADS data set: The budgets of heat, buoyancy and turbulent kinetic energy at the surface of the global ocean. Tech. Rep. 15, Max Plank Institute, Hamburg, Germany, 20 pp.
- Parthasarathy, B., A. A. Munot, and D. R. Kothawale, 1994: All-India monthly and seasonal rainfall series: 1871–1993. *Theor. Appl. Climatol.*, **49**, 219–224.
- Reynolds, R. W., 1988: A real time global sea surface temperature analysis. *J. Climate*, **1**, 75–86.
- , and D. C. Marisco, 1993: An improved real time global sea surface temperature analysis. *J. Climate*, **6**, 114–119.
- Saji, N. H., B. N. Goswami, P. N. Vinayachandran, and T. Yamagata, 1999: A dipole mode in the tropical Indian Ocean. *Nature*, **401**, 360–363.
- Schott, F. A., and J. P. McCreary Jr., 2001: The monsoon circulation of the Indian Ocean. *Progress in Oceanography*, Vol. 51, Elsevier, 1–123.
- Smith, T. M., and R. W. Reynolds, 2004: Improved extended reconstruction of SST (1854–1997). *J. Climate*, **17**, 2466–2477.
- Terray, P., 1995: Space-time structure of monsoon interannual variability. *J. Climate*, **8**, 2595–2619.
- Trenberth, K. E., and A. Solomon, 1994: The global heat balance: Heat transports in the atmosphere and ocean. *Climate Dyn.*, **10**, 107–134.
- Vranes, K., A. L. Gordon, and A. Field, 2002: The heat transport of the Indonesian Throughflow and implications for the Indian Ocean heat budget. *Deep-Sea Res.*, **50**, 1391–1410.
- Wacongne, S., and R. C. Pacanowski, 1996: Seasonal heat transport in the tropical Indian Ocean. *J. Phys. Oceanogr.*, **26**, 2666–2699.
- Wajcovicz, R., and P. S. Schopf, 2001: Oceanic influences on the seasonal cycle in evaporation over the Indian Ocean. *J. Climate*, **14**, 1199–1226.
- Webster, P. J., V. Magaña, T. N. Palmer, J. Shukla, R. Tomas, T. M. Yanai, and T. Yasunari, 1998: The monsoon: Processes, predictability and the prospects for prediction. *J. Geophys. Res.*, **103**, 14 451–14 510.
- , J. P. Loschnigg, A. Moore, and B. Leben, 1999: The great Indian Ocean warming of 1997–1998: Evidence of coupled oceanic-atmospheric instabilities. *Nature*, **401**, 356–360.
- , and Coauthors, 2002a: The Joint Air-Sea Monsoon Interaction Experiment (JASMINE) pilot study. *Bull. Amer. Meteor. Soc.*, **83**, 1603–1630.
- , C. Clark, G. Chirokova, J. Fasullo, W. Han, J. Loschnigg, and K. Sahami, 2002b: The monsoon as a self-regulating coupled ocean-atmosphere system. *Meteorology at the Millennium*, R. P. Pearce, Ed., Academic Press, 198–219.
- Yasunari, T., 1991: The monsoon year—A new concept of the climatic year in the Tropics. *Bull. Amer. Meteor. Soc.*, **72**, 1331–1338.
- Yu, L., and M. M. Rienecker, 1999: Mechanisms for the Indian Ocean warming during the 1997–98 El Niño. *Geophys. Res. Lett.*, **45**, 735–738.
- , and —, 2000: Indian Ocean warming of 1997–1998. *J. Geophys. Res.*, **105**, 16 923–16 939.